ARTICLE

OBC
www.rsc.org/obc

Experimental charge density of a potential DHO synthetase inhibitor: dimethyl-*trans*-2-oxohexahydro-pyrimidine-4,6-dicarboxylate†

David E. Hibbs,*[a] Jacob Overgaard,[b] Siân T. Howard[a] and Thanh Ha Nguyen[a]
[a] *Faculty of Pharmacy, University of Sydney, NSW 2006, Australia*
[b] *School of Chemistry, University of Sydney, NSW 2006, Australia*

Received 20th October 2004, Accepted 8th December 2004
First published as an Advance Article on the web 5th January 2005

The experimental charge density distribution of dimethyl-*trans*-2-oxohexahydro-pyrimidine-4,6-dicarboxylate **1** has been determined using single-crystal X-ray diffraction data measured at 100 K, in terms of the rigid-pseudoatom formalism. Multipole refinement converged at $R(F) = 0.034$ for 7283 reflections with $I > 3\sigma(I)$ and $\sin\theta/\lambda \leq 1.13$ Å^{-1}. Covalent and hydrogen bonding interactions are analyzed using a topological analysis of the Laplacian of the charge density. The experimentally derived electrostatic potential mapped onto the reactive surface of the molecule reveals the potential binding sites of **1**.

Introduction

In recent years it has been established that the *de novo* biosynthesis of pyrimidine nucleotides is initiated by a trifunctional protein called DHO synthetase. One part of this enzyme is dihydroorotase, which acts as a catalyst in the conversion of *N*-carbamoyl-L-aspartate to L-dihydroorotate in the third step of this cascade of reactions. It has been recognised in the treatment of malaria that these parasites, in contrast to humans, can only obtain pyrimidine nucleotides by the *de novo* biosynthesis[1] and the inhibition of this pathway would potentially be the recipe towards a successful anti-malarial drug.[2]

It has been shown that the active site of dihydroorotase contains a bound zinc atom.[3] Scheme 1 has been proposed,[4,5] in which the zinc atom stabilises a tetrahedral transition state in the substrate.

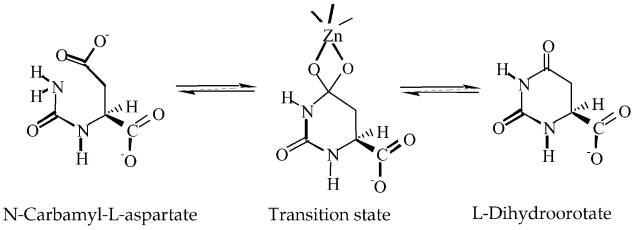

Scheme 1

To investigate the potential for inhibiting the function of dihydroorotase, a number of 'transition state inhibitors' have been synthesized based on the possible mechanism shown in Scheme 1 and some are effective inhibitors of the enzyme.[6] A selection of these inhibitors, among these *trans*-2-oxo-hexahydropyrimidine-4,6-dimethoxycarboxylate or HTDP, were subsequently crystallized and their molecular structures elucidated using X-ray crystallography.[7] These studies emphasized the importance of the hydrogen bonding capabilities of the exocyclic carbonyl oxygen atom as well as those of the two ester groups.

This paper describes the experimental and theoretical charge density (CD) study of HTDP **1** which has a network of hydrogen bonds in the crystalline state. Unlike gas-phase quantum-chemical calculations, the experimental electron density per definition incorporates essential effects such as those from a crystal field and electron correlation,[8] so in principle it can provide a more precise and realistic picture of the molecular charge distribution. By analyzing the hydrogen bonds in a quantitative manner, we might hope to draw conclusions with respect to the non-covalent interactions in the inhibitor–enzyme complex. In particular, emphasis will be placed on the topological analysis of the electron density using the Atoms in Molecules (AIM) theory pioneered by Bader.[9] To further evaluate the ability of the drug to interact with the enzyme, the electrostatic potential calculated on a specific molecular surface will identify the regions that are most likely to interact. This avenue of research has been explored by Politzer and Murray who, using theoretical calculations, have obtained remarkable correlations between electrostatic characteristics and molecular properties.[10]

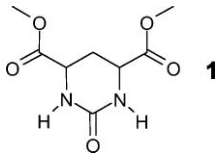
1

Results and discussion

Details of the final statistics of fit for the 7283 reflections used in the multipole refinement are given in Table 1; atom labelling is shown in Fig. 1. Bond lengths and angles from this work are given in Table 2, along with those from a previous crystal structure analysis[7] and the B3LYP/6-311++G** optimized structure.

CCDC reference number 253413. See http://www.rsc.org/suppdata/ob/b4/b416118a/ for crystallographic data in .cif or other electronic format.

A careful CD study usually takes into account the rigid-bond test of Hirshfeld[11] as a check of the thermal parameters obtained from the refinement. Hirshfeld's upper limit for the component of the mean-square displacement of any atom in the directions of all bonds to that atom is 0.001 Å^2 for atoms as least as heavy as carbon. The highest value obtained in this study was 0.0007 Å^2 for N(1)–C(4). The rigid bond test is therefore satisfied, lending credibility to our model and to the quality of the diffraction data.

† Electronic supplementary information (ESI) available: structure factors, full tables of bond lengths and angles, along with multipole coefficients and local coordinate systems. See http://www.rsc.org/suppdata/ob/b4/b416118a/

DOI: 10.1039/b416118a

Table 1 Experimental data for HDTP

Chemical formula	$C_8H_{12}N_2O_5$
Chemical formula weight	216.20
Cell setting	Triclinic
Space group	$P\bar{1}$
a/Å	7.4377(2)
b/Å	8.3035(2)
c/Å	9.2515(3)
α/°	73.265(2)
β/°	67.994(2)
γ/°	71.219(2)
V/Å^3	492.34(2)
D_x/Mg m^{-3}	1.458
Radiation	MoKα
Wavelength/Å	0.71073
Theta range/°	2.42–53.63
μ/mm^{-1}	0.122
Temperature/K	100(2)
Crystal form	Block
Crystal size/mm	0.40 × 0.40 × 0.45
Crystal colour	Colourless
Data collection	
Diffractometer	Bruker AXS CCD
Absorption correction	SADABS
T_{min}	0.7252
T_{max}	1.0000
No. of measured reflections	13998
No. of independent reflections	9273
No. of observed reflections	7283
$R_{(int)}$	0.014
θ_{max}/°	53.63
Intensity decay	None
Refinement	
N (IAM, multipole)	185, 347
$R(F)$	0.051, 0.034
$R_w(F)$	0.046, 0.028
S	1.06, 3.76

N = No. of Refined Parameters; $R = \Sigma\,|F_o| - |F_c|/\Sigma\,|F_o|$; $R_w = [\Sigma w(|F_o| - |F_c|)^2/\Sigma w|F_o|^2]^{1/2}$; $S = [\Sigma w(|F_o| - |F_c|)^2/(M - N)]^{1/2}$, M = No. of observations.

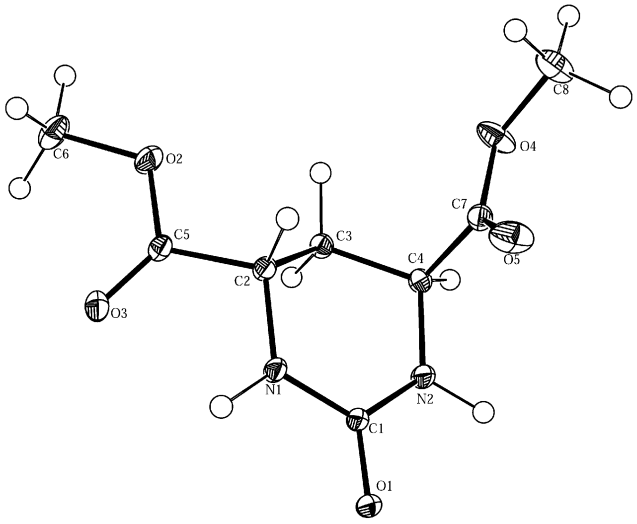

Fig. 1 Thermal ellipsoids plot showing the atom labelling. The ellipsoids depict the 50% probability surface from the final multipole refinement.

Molecular structure

The structure consists of neutral molecules of *trans*-HTDP with a number of intermolecular hydrogen bonds (HBs), the strongest being between the amino hydrogen atoms H(01) and H(02) and the exocyclic oxygen O(1). Although the differences between the DFT gas-phase optimized geometry and the X-ray structure from this work are generally small, there is one notable exception which is the O(1)–C(1) bond length—0.034 Å longer in the crystal. This difference presumably quantifies the extent to which this carbonyl bond is stretched by its participation in a strong intermolecular H-bond. We note that the ester groups incorporating C(5) and C(7) are equatorial and axial to the ring, respectively.

Table 2 Selected bond lengths (Å) and angles (°)

	This work	Gas-phase DFT
O(1)–C(1)	1.2544(7)	1.220
O(2)–C(5)	1.3367(7)	1.344
O(2)–C(6)	1.4533(8)	1.444
O(3)–C(5)	1.2110(9)	1.205
O(4)–C(7)	1.3409(8)	1.347
O(4)–C(8)	1.4486(9)	1.443
O(5)–C(7)	1.2080(9)	1.204
N(1)–C(1)	1.3607(6)	1.374
N(1)–C(2)	1.4542(6)	1.446
N(2)–C(1)	1.3581(6)	1.386
N(2)–C(4)	1.4448(6)	1.446
C(2)–C(3)	1.5291(6)	1.534
C(2)–C(5)	1.5220(6)	1.525
C(3)–C(4)	1.5321(6)	1.541
C(4)–C(7)	1.5317(7)	1.538
C(5)–O(2)–C(6)	116.38(6)	116.1
C(7)–O(4)–C(8)	115.59(6)	116.2
C(1)–N(1)–C(2)	123.53(4)	124.3
C(1)–N(2)–C(4)	124.23(4)	126.1
O(1)–C(1)–N(1)	120.84(5)	122.8
O(1)–C(1)–N(2)	121.01(5)	121.6
N(1)–C(1)–N(2)	118.08(4)	115.5
N(1)–C(2)–C(3)	110.17(4)	109.1
N(1)–C(2)–C(5)	108.70(4)	109.3
C(3)–C(2)–C(5)	110.79(4)	113.5
C(2)–C(3)–C(4)	109.95(4)	109.5
N(2)–C(4)–C(3)	110.87(4)	109.6
N(2)–C(4)–C(7)	111.03(4)	112.7
C(3)–C(4)–C(7)	110.72(4)	109.8
O(2)–C(5)–O(3)	124.95(6)	124.3
O(2)–C(5)–C(2)	111.21(5)	111.1
O(3)–C(5)–C(2)	123.85(5)	124.6
O(4)–C(7)–O(5)	124.23(7)	124.2
O(4)–C(7)–C(4)	110.50(5)	110.3
O(5)–C(7)–C(4)	125.28(6)	125.5

Charge density distribution

The maximum residual peak and trough seen at completion of this refinement was 0.291 and −0.317 e Å^{-3}, respectively. It is clear from the difference Fourier maps (Fig. 2), based on all available data, that there is no significant unmodelled density, a condition for a successful multipole description. There are also no significant features in the residual density of the other ester group, so it is not shown here.

The function $L(\boldsymbol{r}) = -\nabla^2\rho(\boldsymbol{r})$, which was first used as a tool for analyzing densities obtained from quantum-chemical molecular calculations,[9] has now been widely adopted for displaying the 'static' electron density (*i.e.* with thermal motion deconvoluted) in experimental charge density analyses. Unlike the various possible deformation densities[8] it does not depend on a choice of reference density. It clearly identifies regions of local charge concentration and depletion associated with bond formation, and moreover provides a simple classification scheme whereby open-shell (covalent) interactions are characterized by ($L(\boldsymbol{r}) > 0$) and closed-shell (ionic) interactions ($L(\boldsymbol{r}) < 0$). Fig. 3 depicts $L(\boldsymbol{r})$ in the plane of the N(C=O)N moiety of **1**, with the experimental density in the upper panel and the gas-phase DFT density in the lower panel for comparison. The dark shaded areas delineate the so-called valence shell of charge concentration (VSCC).

Some differences are evident: (i) the shape of the carbonyl oxygen valence shell, which is more extended in the experimental density; (ii) the VSCC is more 'pinched' in the carbonyl bond of the experimental density; (iii) the VSCC is continuous from N1–C1–N2 in the experimental density. Since this oxygen atom

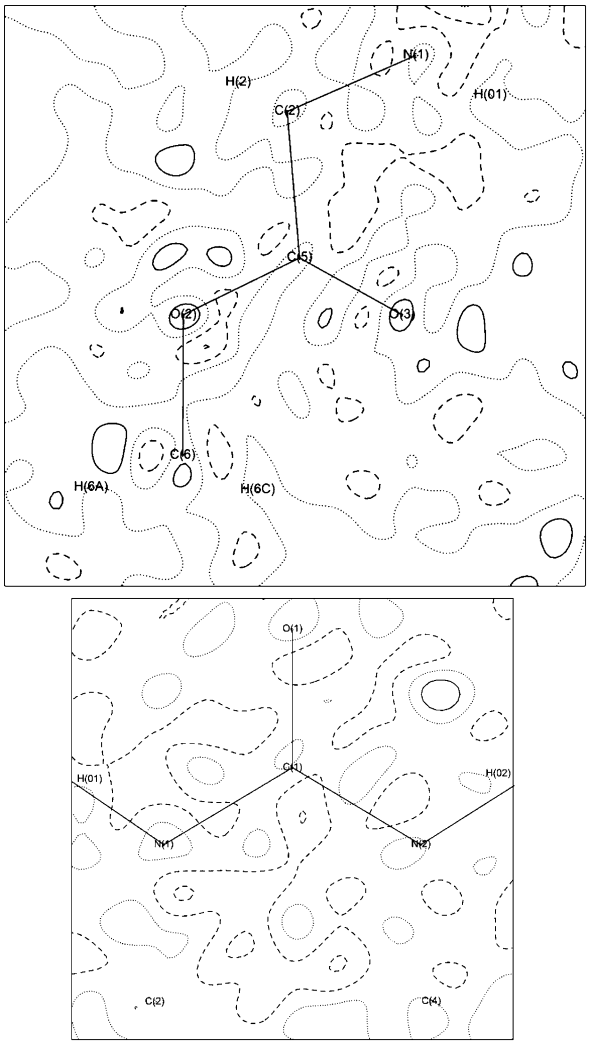

Fig. 2 Residual density maps in (upper) the plane of the ester group incorporating C(5) and (lower) the NC(=O)N group of the pyrimidine ring. The solid lines show positive contours and the dashed lines show negative contours, both incremented by 0.1 e Å^{-3}. The zero contour is shown as a dotted line.

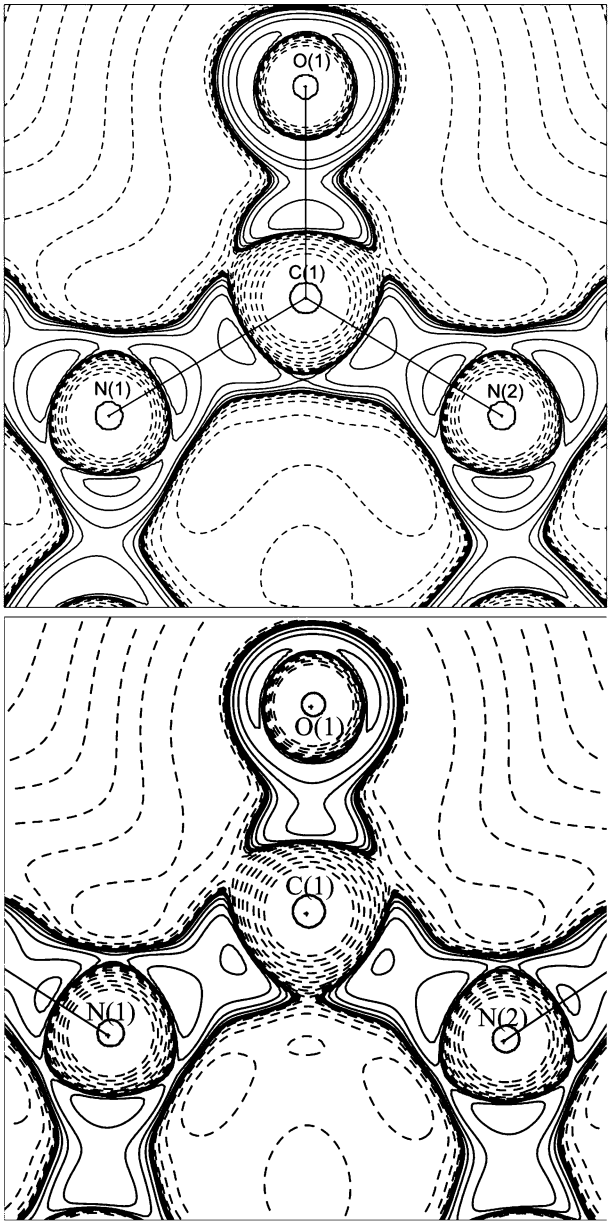

Fig. 3 $-\nabla^2\rho$ Distribution in the plane of the NC(=O)N group of the pyrimidine ring: (upper) from multipole refinement, (lower) from DFT gas-phase theory. Contours shown are ±2, 4, 8 × 10^n, $n = -3, -2, -1, 0, 1, 2$ e Å^{-5} with solid lines representing negative contours and dashed lines positive contours.

is involved in hydrogen bonding, all these differences might in principle be due to the presence of this interaction which is absent in the gas-phase calculation.

Fig. 4 shows the corresponding $L(\boldsymbol{r})$ distributions in the plane of one of the ester groups. Although the carbonyl oxygen here is not involved in hydrogen bonding, we see two of the same key differences in comparison with the DFT-derived density: the continuous VSCC from C2–C5–O2; and the more pinched VSCC in the carbonyl bond. The latter effect suggests a more ionic character for the carbonyl bonds in the experimental density.

Topological analysis

Table 3 summarizes the bond critical point (bcp) properties—these are the values of the functions ρ and $-\nabla^2\rho$ at the points $\{\boldsymbol{r}_c\}$ in the bond (where $\nabla\rho(\{\boldsymbol{r}_c\}) = 0$).[9] The topological analysis of the electron density confirms the existence of covalent interactions in all C–O bonds in the structure (see Table 3) as all bonds show positive values of $L(\boldsymbol{r})$ at the bcp. There are some systematic trends to note in Table 3 concerning the comparison between experiment and theory. Firstly, the DFT values of ρ at the bcp are lower than experiment by up to 13%, the largest deviations occurring in the polar bonds. This trend, frequently observed in charge density studies,[12] is normally associated with a difference in the distance of the bcp in the theoretical density from the more electronegative atom (see column $d_{1\ -bcp}$), and the same explanation appears to apply to the data presented here.

The values of ρ_b and $-\nabla^2\rho_b$ evaluated at bcps in the three pairs of chemically identical CO bonds and the two pairs of chemically identical CC bonds are reassuringly very similar in the experimental density (average differences in $\rho_b = 0.03$ e Å^{-3}) despite that fact that no chemical constraints have been applied during multipole refinement. Also the {C2–N1, C4–N2} pair of bonds have the same ρ_b value to within 0.01 e Å^{-3}. However, ρ_b in the pair of bonds {C1–N1, C1–N2} differs by 0.10 e Å^{-3}, despite the fact that the bonds differ in length by only 0.003 Å. This difference could indeed be indicative of the asymmetric intermolecular H-bond interactions in which the atoms N1, C1 and C2 are all participating, to be discussed in more detail shortly.

Hydrogen bond analysis

The crystal structure of **1** exhibits a variety of HBs. The exocyclic carbonyl O(1) atom is hydrogen bonded to two co-planar

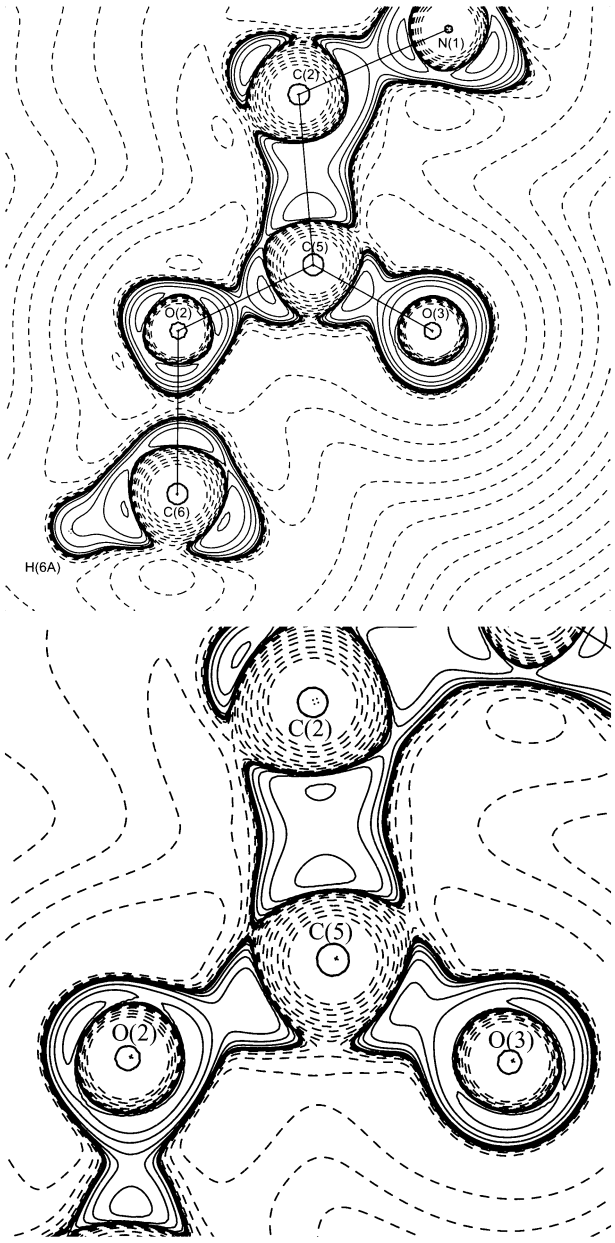

Fig. 4 $-\nabla^2\rho$ Distribution in the plane of an ester group: (upper) experimental, multipole refined; (lower) from DFT gas-phase theory. Contours as in Fig. 3.

molecules through N(1)–H(01) and N(2)–H(02), respectively. This creates an infinite chain of molecules bound by relatively strong interactions (O···H distances 2.06 Å and 1.92 Å, respectively). In addition, the three-dimensional lattice is built from a much longer N–H···O contact involving an ester oxygen and two still weaker C–H···O interactions. Among these weaker HBs, O(5)···H(2)^{iii}–C(2)^{iii} is responsible for forming a dimer perpendicular to the chain formed by the stronger HBs. On the opposite side of the chain, another dimer is formed *via* the O(3)···H(3B)^{iv}–C(3)^{iv} HB. In Table 4 we also report the HB energies using the simple formula derived from the combined works of Abramov[13] and Espinosa *et al.*[14]

$$E_{HB} = 25.0 \times 10^3 \exp[-3.6r(H\cdots O)]\ \text{kJ mol}^{-1}$$

This suggests that the shorter contact HB with $r(O\cdots H) =$ 1.92 Å is about 60% stronger than the HB with $r(O\cdots H) =$ 2.06 Å, and furthermore that the remaining HB's have very small energies $\leq$5 kJ mol^{-1}. In fact all the HBs classify as weak according to the scheme by Hibbert and Emsley.[15]

Fig. 5 depicts $-\nabla^2\rho$ in the plane of the density in the HB N(1)–H(01)···O(1). The HB doesn't appear to produce any noticeable polarization of oxygen lone pair (LP) density in the hydrogen-bonding direction. Table 4 also contains an entry for a weak intramolecular HB with very bent geometry. This HB creates a five-membered ring, and a corresponding ring-critical point is found at the centre. No analogous hydrogen bond CP or ring-critical point CP could be located in the single-point DFT density.

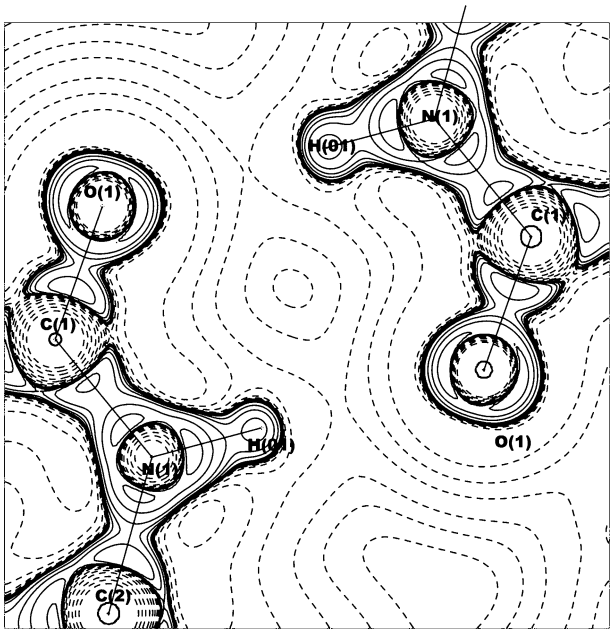

Fig. 5 $-\nabla^2\rho$ Distribution in the N(1)–H(01)···O(1) hydrogen bond. Contours as in Fig. 3.

Lone pair analysis

A topological analysis of $\nabla^2\rho$ locates stationary points (*i.e.* $\nabla(\nabla^2\rho) = 0$) where the concentration of charge density is maximal; these occur both in bonds and LPs. The LP peaks for oxygen atoms involved in HBs have been analyzed in some detail using MP2-level calculations.[16] Table 5 shows the relevant details for the pairs of LPs in the VSCCs located around the five oxygen atoms in **1**, and compares them with the equivalent results from the gas-phase DFT calculation. The experimental EDD does not display two separate LPs on the two methoxy oxygen atoms; instead a broad region of negative $\nabla^2\rho$ with a single maximum covers the entire face of these oxygens, as shown in Fig. 6. This is not an artefact of the experimental density since it is also found in the DFT density. There is no previous report of this feature of methoxy oxygen atoms either in experimental or theoretical charge density analysis.

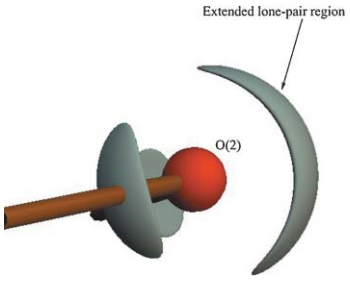

Fig. 6 The 105 e Å^{-5} isosurface in $-\nabla^2\rho$ around O(2).

The oxygen LP centroids are found in a relatively narrow range of radial distances from the oxygen nuclei which are in excellent agreement between experiment (0.337 Å $< r_{LP} <$ 0.345 Å) and gas-phase DFT theory (0.342 Å $< r_{LP} <$ 0.345 Å). It is noteworthy that the O(1) oxygen which is involved in two

Table 3 Topological analysis of **1**. [ρ_b] in e Å^{-3}; [$\nabla^2\rho_b$] in e Å^{-5}; R_{1-2} and d in Å

Bond	Model[a]	ρ_b	$-\nabla^2\rho_b$	ε	R_{1-2}	d_{1-bcp}	d_{2-bcp}
O(1)–C(1)	Exp	2.86(1)	34.31(7)	0.10	1.255	0.803	0.451
	DFT	2.77	10.2	0.09	1.220	0.798	0.422
O(2)–C(5)	Exp	2.29(1)	24.74(6)	0.07	1.337	0.845	0.492
	DFT	2.04	11.4	0.01	1.344	0.880	0.464
O(2)–C(6)	Exp	1.69(1)	6.34(3)	0.05	1.454	0.849	0.605
	DFT	1.57	7.1	0.00	1.444	0.946	0.498
O(3)–C(5)	Exp	3.10(2)	15.71(9)	0.16	1.211	0.807	0.404
	DFT	2.82	3.5	0.07	1.205	0.793	0.412
O(4)–C(7)	Exp	2.32(1)	23.37(6)	0.06	1.341	0.830	0.511
	DFT	2.02	11.2	0.02	1.347	0.882	0.466
O(4)–C(8)	Exp	1.72(1)	6.72(4)	0.06	1.449	0.850	0.599
	DFT	1.57	7.3	0.00	1.443	0.945	0.499
O(5)–C(7)	Exp	3.06(2)	14.56(9)	0.13	1.208	0.801	0.407
	DFT	2.82	3.2	0.00	1.204	0.793	0.412
N(1)–C(1)	Exp	2.26(1)	24.78(4)	0.19	1.361	0.832	0.529
	DFT	2.12	22.5	0.16	1.374	0.846	0.529
N(1)–C(2)	Exp	1.82(1)	10.15(3)	0.09	1.455	0.833	0.622
	DFT	1.82	17.5	0.07	1.447	0.868	0.578
N(2)–C(1)	Exp	2.36(1)	27.59(4)	0.19	1.359	0.840	0.519
	DFT	2.07	21.8	0.15	1.386	0.848	0.578
N(2)–C(4)	Exp	1.82(1)	10.82(3)	0.09	1.445	0.843	0.602
	DFT	1.81	17.3	0.04	1.446	0.869	0.577
C(2)–C(3)	Exp	1.65(1)	9.56(2)	0.04	1.529	0.795	0.735
	DFT	1.63	13.1	0.02	1.534	0.782	0.752
C(2)–C(5)	Exp	1.72(1)	11.94(2)	0.17	1.522	0.701	0.821
	DFT	1.71	14.8	0.09	1.525	0.737	0.788
C(3)–C(4)	Exp	1.65(1)	9.23(2)	0.05	1.532	0.748	0.784
	DFT	1.60	12.6	0.02	1.541	0.753	0.788
C(4)–C(7)	Exp	1.77(1)	12.09(2)	0.13	1.532	0.740	0.792
	DFT	1.68	14.1	0.09	1.538	0.738	0.800

[a] The abbreviations Exp and DFT represent experimentally determined and DFT at the optimised geometry, respectively.

Table 4 Experimental geometrical and bond-topological parameters for hydrogen bonds

A···H–D[a]	r(A···D)[b]/Å	r(A···H)/Å	a(A···H–D)/°	ρ_b/e Å^{-3}	$\nabla^2\rho_b$/e Å^{-5}	r(A–CP)/Å	λ_3/e Å^{-5}	E_{HB}/kJ mol^{-1}
O(1)···H(02)^{i}–N(2)^{i}	2.92	1.92	172.1	0.15(1)	2.81	1.25	4.22	24.9
O(1)···H(01)^{ii}–N(1)^{ii}	3.06	2.06	170.8	0.10(1)	2.00	1.32	2.88	15.0
O(3)···H(01)–N(1)	2.69	2.48	90.6	0.06(1)	1.63	1.36	2.04	3.3
O(5)···H(2)^{iii}–C(2)^{iii}	3.44	2.36	167.5	0.06(1)	1.07	1.44	1.51	5.1
O(3)···H(3B)^{iv}–C(3)^{iv}	3.50	2.67	132.9	0.05(1)	0.59	1.56	0.90	1.7

[a] i $2-x, -y, 1-z$; ii $1-x, -y, 1-z$; iii $1-x, -y, 2-z$; iv $1-x, 1-y, 1-z$. [b] r(A···H) and r(A···D) are the distances of the acceptor atoms from the hydrogen atom and from the donor atom, respectively. a(A···H–D) is the angle formed by the acceptor, hydrogen and donor atoms.

Table 5 Non-bonded valence shell charge concentrations around the oxygen atoms

Atom	Type of CP	Model	$-\nabla^2\rho$/e Å^{-5}[a]		r_{LP}/Å[b]		C–O–LP/°[c]	
O(1)	(3, −3) in $\nabla^2\rho$	Exp	136.7	135.7	0.339	0.339	106.9	102.9
		DFT	111.8	111.5	0.345	0.345	107.5	107.3
O(2)	(3, −3) in $\nabla^2\rho$	Exp	114.8		0.342		120.3	
		DFT	117.9		0.342		120.6	
O(3)	(3, −3) in $\nabla^2\rho$	Exp	126.0	115.6	0.341	0.343	113.1	113.4
		DFT	117.7	118.2	0.343	0.343	109.3	107.7
O(4)	(3, −3) in $\nabla^2\rho$	Exp	144.6		0.340		113.2–131.2	
		DFT	118.1		0.342		120.7–113.2	
O(5)	(3, −3) in $\nabla^2\rho$	Exp	154.4	157.5	0.337	0.337	126.5	97.9
		DFT	117.6	118.9	0.343	0.342	109.1	107.8

[a] $-\nabla^2\rho$ at the lone pair centroid. [b] Distance from nucleus to LP centroid. [c] Angle between the C–O internuclear vector and the LP···(O nucleus) vector.

strong HBs has the smallest pair of C=O···LP angles (average 104.9°)—this angle would be 120° for formal sp^2 hybridization. The O–LP···H angles are 164.5° and 156.2° to H(02) and H(01), respectively, *i.e.* together with the H···LP distances of 1.745 Å to H(01) and 1.591 Å to H(02), this corroborates the inferences from geometrical and ρ-topological analyses that N(2)–H(02)···O(1) is stronger than N(1)–H(01)···O(1). It is also clear, from the analysis of the two weaker HBs perpendicular to the chain, that the C(3)–H(3B)···O(3) is weaker than the C(2)–H(2)···O(5) HB, with O–LP···H angles and H···LP distances of 103.3° and 2.57 Å, and 153.7° and 2.05 Å, respectively for H(3B) and H(2). The angular disposition of the LP does therefore appear to play a role in determining HB strength.

Table 6 Atomic charges

Ω	$q_{exp}(\Omega)$	$q(P_v)$	$q_{dft}(\Omega)$
O(1)	−1.227	−0.298	−1.171
O(2)	−1.015	−0.280	−1.061
O(3)	−1.303	−0.192	−1.137
O(4)	−1.063	−0.298	−1.010
O(5)	−1.349	−0.288	−1.140
N(1)	−1.222	−0.543	−1.111
N(2)	−1.224	−0.530	−1.087
C(1)	+1.901	+0.173	+1.796
C(2)	+0.200	+0.001	+0.370
C(3)	−0.208	−0.298	+0.050
C(4)	+0.132	−0.055	+0.384
C(5)	+1.622	−0.102	+1.525
C(6)	+0.021	−0.338	+0.438
C(7)	+1.516	−0.112	+1.490
C(8)	+0.111	−0.318	+0.438
H(01)	+0.607	+0.417	+0.424
H(02)	+0.598	+0.417	+0.399
H(2)	+0.166	+0.284	+0.042
H(3A)	+0.127	+0.223	+0.040
H(3B)	+0.106	+0.223	+0.026
H(4)	+0.199	+0.284	+0.044
H(6A)	+0.234	+0.271	+0.042
H(6B)	+0.215	+0.271	+0.048
H(6C)	+0.235	+0.271	+0.049
H(8A)	+0.186	+0.271	+0.044
H(8B)	+0.219	+0.271	+0.042
H(8C)	+0.216	+0.271	+0.049

Atomic charges

One way to derive atomic charges from multipole refinement which are directly comparable with theoretical results is to determine the 'interatomic surfaces' with normal vectors $\boldsymbol{n}$ ($\nabla\rho\cdot\boldsymbol{n} = 0$) and to then integrate the charge density over the 'atomic basins' defined by these surfaces.[9] Table 6 reports atomic charges derived in this way, as well as the monopole charges: $q(P_{v,j}) = Z_j - P_{v,j}$, where Z_j is the atomic number, and $P_{v,j}$ is multipole-refined population in the Hartree–Fock monopole on the jth atom. There is an excellent correlation between the experimental and gas-phase DFT values of $q(\Omega)$—both showing a larger negative charge on the carbonyl oxygen atoms than on the methoxy oxygens. Pairs of charges corresponding to chemically identical atoms are again reassuringly similar *e.g.* (−1.30 *versus* −1.35) for the two ester carbonyl oxygen atoms; (−1.02 *versus* −1.06) for the two methoxy oxygens; and (−1.22 *versus* −1.22) for the two nitrogens. Both theory and experiment give a highly electropositive C(1), significantly more positive than the carbon atoms of the ester groups.

Electrostatic potential

The multipole description of the experimental electron density enables the calculation of the molecular electrostatic potential (MEP)[8] for a molecule 'removed' from the crystal (although the refined multipole parameters implicitly contain crystal field effects). The MEP is especially important with respect to non-covalent interactions in drug-receptor studies, in addition to steric requirements, dispersive interactions *et cetera*. The required complementarity of the drug and receptor electrostatic environments[17] make the MEP a key feature in drug design.

There are numerous ways to display and/or and characterise the EP, however, but the mapping of the EP on the molecular reactive surface has proved particularly useful in QSAR models of physical properties.[18] Here we focus on a few features of the experimental MEP based on the appearance of the 0.001 a.u. isodensity surface map displayed in Fig. 7.

(i) The darker intensity of blue around O(1) demonstrates that a test positive charge would bind more strongly here than at any of the ester oxygens. This is despite the fact that the $q(\Omega)$ charges are actually more negative for O(3) and O(5), *i.e.* key contributions to the MEP are coming from higher multipoles ($l > 0$). This is all consistent with the fact that the two strongest HBs in the crystal involve O(1).

(ii) Both O(2) and O(4) in the methoxy ester groups are unlikely to form HBs with the receptor, given the more-or-less zero value of the MEP on the 0.001 a.u. surface.

(iii) Surprisingly, the red colour of the MEP surrounding the hydrogens of the two methyl groups suggests that this is a possible H-bond interaction site with a receptor.

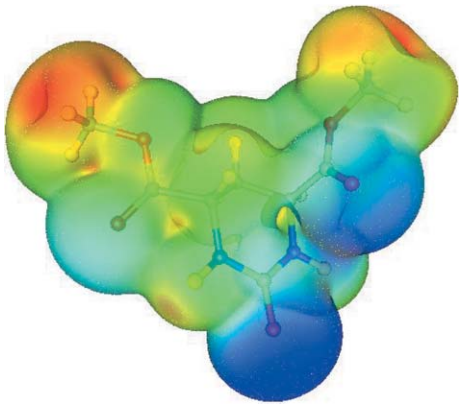

Fig. 7 Experimental electrostatic potential of **1** on the 0.001 a.u. isodensity surface. A color gradient is applied to show the change from electronegative regions (blue) over neutral (green) to electropositive (red).

Conclusions

An experimental charge density of a potential DHO synthetase inhibitor has been obtained from a dataset with excellent merging statistics ($R_{int} = 0.014$) for symmetry-equivalent reflections. The near-equivalence of chemically identical groups in the molecule, along with excellent agreement between experiment and gas-phase DFT, confirms that the multipole-refined density is of high-quality. An analysis of $\nabla^2\rho$ for the lone pair regions of oxygen atoms involved in hydrogen bonds finds maxima closely aligned with the hydrogen bond direction only in the case of the stronger hydrogen bonds. The electrostatic potential mapped on to the 0.001 a.u. isodensity surface of a molecule removed from the crystal suggests that, as in the crystal structure, strong H-bonds would be likely to form with a receptor and the carbonyl oxygen of the N–(C=O)–N moiety, while weaker C–H···O hydrogen bonds involving one or more terminal methyls of the two methoxy ester groups and a receptor are also possible.

Experimental

The preparation of HTDP has been described elsewhere.[4] Crystals were obtained from non-aqueous solvents by slow evaporation.

X-Ray data collection

Single-crystal, high-resolution, low-temperature data were collected on a Bruker SMART 1000 CCD based diffractometer. Cell constants were obtained from the least-squares refinement of 4204 reflections located between 5.3 and 106.9° 2θ. Two reciprocal space data spheres were collected, with one sphere providing data between 0 and 56° in 2θ, and a second for data between 54 and 110° in 2θ. Data were collected at 100(2) K with χ-scan increments of 0.3°. The intensities of 324 reflections recollected at the end of the experiment did not change significantly during data collection. An empirical data correction determined with SADABS[19] was applied to the data. The data integration and reduction were undertaken with SAINT and XPREP.[20]

Molecular orbital calculations

Quantum chemical calculations were performed with the GAUSSIAN98 program package[21] at the B3LYP/6-311++G** level of theory. A full optimisation was carried out starting with the X-ray structural data, followed by a harmonic vibrational frequency calculation which verified that a stable minimum energy conformer has been obtained. Topological analyses of ρ and $\nabla^2\rho$ were also carried out on wave functions obtained from single point calculations using the experimental (in-crystal) coordinates, and employed the AIMPAC suite of programs.[22]

Multipole refinement

The crystal structure determination was determined in an earlier publication.[7] The structural parameters therein formed the starting point for a high-order independent atom model (IAM) refinement to determine non-hydrogen atom nuclear coordinates (subsequently fixed in multipole refinement). Refinements were carried out using the full-matrix least-squares program XDLSM of the XD program package,[23] which utilizes the rigid pseudoatom model[24] in the formalism proposed by Hansen and Coppens.[25] For all refinements the quantity $\Sigma_{\boldsymbol{H}} w_{\boldsymbol{H}}(|F_{\rm obs}(\boldsymbol{H})| - k|F_{\rm calc}(\boldsymbol{H})|)^2$ was minimised with the weight $w_{\boldsymbol{H}} = 1/\sigma^2(F_{\rm obs}(\boldsymbol{H}))$, using the subset of structure factors with $F_{\rm obs}(\boldsymbol{H}) > 3\sigma(F_{\rm obs}(\boldsymbol{H}))$.

In multipole analysis the electron density $\rho(\boldsymbol{r})$ can be described by as a superposition of contributions from aspherical 'pseudoatoms', $\rho(\boldsymbol{r}) = \Sigma_j\, \rho_j(\boldsymbol{r} - \boldsymbol{R}_j)$ which have nuclear positions $\{\boldsymbol{R}_j\}$. The general form of the pseudoatom density is

$$\rho_{\rm j}(\boldsymbol{r}) = P_{\rm c}\rho_{\rm core}(|\boldsymbol{r}|) + \kappa'^3 P_{\rm v}\rho_{\rm v}(\kappa'|\boldsymbol{r}|) + \sum_{l=0}^{3} \kappa''^3 R_l(\kappa''|\boldsymbol{r}|) \sum_{m=-l}^{+l} \kappa''^3 P_{lm} d_{lm}(\boldsymbol{r})$$

thus each pseudoatom is described by three components: core, spherically ymmetric valence, and a set of (aspherical) deformation functions (dipoles, quadrupoles *etc.*). The core and spherical valence density is composed of (squared) Hartree–Fock wave functions expanded in a basis of Slater-type atomic orbitals[26] radially modified by a refinable expansion–contraction parameter κ' (the expansion–contraction coefficient that modifies the radial distribution). The valence monopole population ($P_{\rm v}$) is also refined, whilst the core population parameter ($P_{\rm c}$) is fixed at 2 for first row atoms. The final terms, each with a refinable amplitude P_{lm}, are products of density-normalised spherical harmonics $d_{\rm lmp}$ and Slater type function $R_l(\kappa''|\boldsymbol{r}|) = N_l \boldsymbol{r}^n \exp(-\kappa''\zeta|\boldsymbol{r}|)$ with a second (overall) refined radial parameter κ''. An electroneutrality constraint was applied whereby the overall charge on the molecule was fixed at zero.

In the refinement, the expansion was truncated at the octupolar level ($l_{\rm max} = 3$) for heavy atoms while the asphericity of the hydrogen atoms was modelled with a single bond-directed dipole ($l_{\rm max} = 1$). At this level, the highest coefficient in the variance–covariance matrix was 0.65. Five different sets $\{\kappa', \kappa''\}$ of expansion–contraction parameters were employed: one each for C, N and H atoms, and two sets for the carbonyl and ester oxygens. Hydrogen κ' and κ'' parameters were fixed at 1.2, as suggested by multipole analysis of theoretical densities studies.[27]

Bond lengths to hydrogen atoms were fixed at average neutron diffraction values,[28] with bond directions fixed at values obtained from the IAM refinement and isotropic temperature factors scaled from the refined equivalent isotropic parameter of the parent atom. For RCH_2–H, CHR_2–H, CR_3–H and N–H the bond lengths were 1.074, 1.095, 1.099 and 1.009 Å, respectively.

An isotropic type 2 extinction parameter was refined, giving a domain size of 3×10^{-4} mm. The most affected reflection was 0 −1 2 with 69.3%. The extinction parameter refined to a highly significant value of 0.42(1) and its introduction noticeably improved the residual density maps.

Acknowledgements

We thank R. I. Christopherson for a sample of HDTP, Drs D. Willock (Cardiff), J. Greenwood (Denmark) and J. Hanrahan (Sydney) for use of computational facilities, and the Royal Society for a fellowship (DEH). JO thanks the Danish Research Council for financial support.

References

1 L. W. Scheibel and I. W. Sherman, in *Malaria: Principles and practice in Malariology*, ed. W. H. Wernsdorfer and I. McGregor, Churchill Livingstone, Melbourne, 1988, vol. 1, pp. 234–242.
2 K. K. Seymour, S. D. Lyons, L. Phillips, K. H. Rieckmann and R. I. Christopherson, *Biochemistry*, 1994, **33**, 5268–5274.
3 R. E. Kelly, M. I. Mally and D. R. Evans, *J. Biol. Chem.*, 1986, **261**, 6073–6083.
4 R. I. Christopherson and M. E. Jones, *J. Biol. Chem.*, 1980, **255**, 3358–3370.
5 R. I. Christopherson and S. D. Lyons, *Med. Res. Rev.*, 1990, **10**, 505–548.
6 R. I. Christopherson, K. J. Schmalzl, E. Szabados, R. J. Goodridge, M. C. Harsanyi, M. E. Sant, E. M. Algar, J. E. Anderson, A. Armstrong, S. C. Sharma, W. A. Bubb and S. D. Lyons, *Biochemistry*, 1989, **28**, 463–470.
7 T. W. Hambley, L. Phillips, A. C. Poiner and R. I. Christopherson, *Acta Crystallogr., Sect. B*, 1993, **49**, 130–136.
8 P. Coppens, *X-ray Charge Densities and Chemical Bonding*, Oxford University Press, Oxford, 1997.
9 R. F. W. Bader, *Atoms In Molecules—A Quantum Theory*, Clarendon Press, Oxford, 1990.
10 P. Politzer and J. Murray, *Theor. Chem. Acc.*, 2002, **108**, 134–142.
11 F. L. Hirshfeld, *Acta Crystallogr., Sect. A*, 1976, **32**, 239–247.
12 (*a*) J. Overgaard, M. P. Waller, J. A. Platts and D. E. Hibbs, *J. Phys. Chem. A*, 2003, **107**, 11201–11208; (*b*) T. Koritsanszky, J. Buschmann, D. Lentz, P. Luger, G. Perpetuo and M. Rottger, *Chem. Eur. J.*, 1999, **5**, 3413–3420.
13 Yu. A. Abramov, *Acta Crystallogr., Sect. A*, 1997, **53**, 264–272.
14 E. Espinosa, C. Lecomte and E. Molins, *Chem. Phys. Lett.*, 1998, **285**, 170–173.
15 F. Hibbert and J. Emsley, *Adv. Phys. Org. Chem.*, 1990, 255–379.
16 J. A. Platts, S. T. Howard and B. R. F. Bracke, *J. Am. Chem. Soc.*, 1995, **118**, 2726–2731.
17 Z. Su and P. Coppens, *Acta Crystallogr., Sect. A*, 1992, **48**, 188–195.
18 U. Nornider, in *3D QSAR in drug design*, ed. H. Kubinyi, G. Folkers and Y. C. Martin, Kluwer/Escom, London, Dordrecht, 1998, vol. 3, pp. 3–23.
19 G. M. Sheldrick, *SADABS. Empirical absorption correction program for area detector data*, University of Göttingen, 1996.
20 *SMART, SAINT and XPREP. Area detector control, data integration and reduction software*, Bruker Analytical X-ray Instruments Inc., Madison, Wisconsin, USA, 1995.
21 M. J. Frisch, G. W. Trucks, H. B. Schlegel, G. E. Scuseria, M. A. Robb, J. R. Cheeseman, V. G. Zakrzewski, J. A. Montgomery, Jr., R. E. Stratmann, J. C. Burant, S. Dapprich, J. M. Millam, A. D. Daniels, K. N. Kudin, M. C. Strain, O. Farkas, J. Tomasi, V. Barone, M. Cossi, R. Cammi, B. Mennucci, C. Pomelli, C. Adamo, S. Clifford, J. Ochterski, G. A. Petersson, P. Y. Ayala, Q. Cui, K. Morokuma, D. K. Malick, A. D. Rabuck, K. Raghavachari, J. B. Foresman, J. Cioslowski, J. V. Ortiz, B. B. Stefanov, G. Liu, A. Liashenko, P. Piskorz, I. Komaromi, R. Gomperts, R. L. Martin, D. J. Fox, T. Keith, M. A. Al-Laham, C. Y. Peng, A. Nanayakkara, C. Gonzalez, M. Challacombe, P. M. W. Gill, B. Johnson, W. Chen, M. W. Wong, J. L. Andres, C. Gonzalez, M. Head-Gordon, E. S. Replogle, and J. A. Pople, *Gaussian 98, Revision A.3*, 1998, Gaussian, Inc., Pittsburgh PA.
22 F. W. Biegler-König, R. F. W. Bader and T. H. Tang, *J. Comput. Chem.*, 1982, **3**, 317–352.
23 T. Koritszansky, P. R. Mallinson, S. T. Howard, A. Volkov, P. Macchi, Z. Su, C. Gatti, T. Richter, L. J. Farrugia and N. K. Hansen, *XD—A Computer Program for Multipole Refinement and Analysis of Electron Densities from Diffraction Data*, 2003, Manual Version 12.
24 R. F. Stewart, *Acta Crystallogr., Sect. A*, 1976, **32**, 565–572.
25 N. K. Hansen and P. Coppens, *Acta Crystallogr., Sect. A*, 1978, **34**, 909–921.
26 E. Clementi and C. Roetti, *Atom. Data Nucl. Data Tables*, 1974, **14**, 177–201.
27 S. T. Howard and D. E. Hibbs, unpublished work.
28 F. H. Allen, O. Kennard, D. G. Watson, L. Brammer, A. G. Orpen and R. Taylor, *J. Chem. Soc., Perkin Trans. 2*, 1987, S1–15.